DRAFT IOWTC2019-7578

MACHINE LEARNING-AIDED ASSESSMENT OF WIND TURBINE ENERGY LOSSES DUE TO BLADE LEADING EDGE DAMAGE

Anna Cavazzini[*]
University of Lancaster
Department of Engineering
Lancaster LA1 4YR, United Kingdom

Edmondo Minisci[†]
University of Strathclyde
Department of Mechanical and
Aerospace Engineering
Glasgow G1 1XQ, United Kingdom

M. Sergio Campobasso[‡]
University of Lancaster
Department of Engineering
Lancaster LA1 4YR, United Kingdom

ABSTRACT

Estimating reliably and rapidly the losses of wind turbine annual energy production due to blade surface damage is essential for optimizing maintenance planning and, in the frequent case of leading edge erosion, assessing the need for protective coatings. These requirements prompted the development of the prototype system presented herein, using machine learning, wind turbine engineering codes and computational fluid dynamics to estimate wind turbine annual energy production losses due to blade leading edge damage. The power curve of a turbine with nominal or damaged blade surfaces is determined respectively with the open-source FAST and AeroDyn codes of the National Renewable Energy Laboratory, both using the blade element momentum theory for turbine aerodynamics. The loss prediction system is designed to map a given three-dimensional geometry of a damaged blade onto a damaged airfoil database, which, in this study, consists of 2700+ airfoil geometries, each analyzed with Navier-Stokes computational fluid dynamics over the working range of angles of attack. To avoid the need for lengthy aerodynamic analyses to assess losses due to damages monitored during turbine operation, the airfoil force data of a damaged turbine required by AeroDyn are rapidly obtained using a machine learning method trained using the pre-existing airfoil database. Presented results focus on the analysis of a utility-scale offshore wind turbine and demonstrate that realistic estimates of the annual energy production loss due to leading edge surface damage can be obtained in just a few seconds using a standard desktop computer, highlighting the viability and the industrial impact of this new technology for wind farm energy losses due to blade erosion.

INTRODUCTION

Wind turbine blades often operate in harsh environmental conditions, being exposed to precipitation that occurs in a variety of forms. Over time, rain, hail and airborne abrasive particles such as sand, can erode blade surfaces, particularly at the leading edge. Recent experimental evidence indicates that leading edge erosion reduces significantly the aerodynamic performance of wind turbine blades and, thus, the power plant energy production, by more than 20 % [1, 2]. Significant energy losses due to geometry alterations of the leading edge surface region can also occur due to insect, dust [3] and ice accretion [4].

Previous research efforts to assess the impact of wind turbine in-service blade surface alterations on aerodynamic power losses have focused on the detrimental effect of ice accretion [5], dust [3, 6] and insect debris [7] accumulation, and leading edge roughness [8–10]. Leading edge erosion also results in significant reductions of the lift and large increments of the drag forces, and can thus dramatically reduce the blade performance, particularly in the outboard region, where the relative air speeds are high and most energy capture take place. Despite this, however, the study of the energy losses due to blade erosion has received fairly little attention thus far.

Sareen *et al.* [2] carried out a comprehensive campaign of

---

[*]Email: a.cavazzini@lancaster.ac.uk

[†]Email: edmondo.minisci@strath.ac.uk

[‡]Email: m.s.campobasso@lancaster.ac.uk. Corresponding author.

wind tunnel measurements to assess the aerodynamic performance loss of the DU 96-W-180 wind turbine airfoil subject to geometry alterations due to different patterns (pits, gouges and delamination) and severity (moderate, medium and advanced) of leading edge erosion. Their eroded airfoil design relied on photographic records of wind turbine blades in operation and eroded blades undergoing repair provided by 3M. These photographic data sets collected from wind power plant operators covered a range of rotor blade sizes up to and including megawatt-scale rotors that had been in operation for 1 to 10+ years. Making use of their airfoil force data based on wind tunnel testing, and the PROPID wind turbine analysis and design code, the authors found that the loss of Annual Energy Production (AEP) of a 2.5 MW class turbine due to leading edge erosion can approach 25 % of the nominal value. Schramm *et al.* [11] used OpenFOAM [12], an open-source Navier-Stokes (NS) computational fluid dynamics (CFD) package, and the National Renewable Energy Laboratory (NREL) wind turbine engineering code FAST [13] to assess the impact of a particular leading edge delamination pattern on the AEP of the NREL 5 MW reference turbine [14]. With reference to wind frequency data measured with a met mast at Risø [15], they reported an AEP reduction of about 8 % for the leading edge damage they considered. Wang *et al.* [16] developed a pitting erosion geometric model for the NS CFD analysis of the aerodynamic performance of wind turbine airfoils suffering from this type of surface damage. Each erosion pit was modeled as a semi-circular cavity. Making use of two-dimensional (2D) flow simulations performed with the ANSYS FLUENT incompressible Reynolds-averaged Navier-Stokes (RANS) solver coupled to Menter's $k - \omega$ Shear Stress Transport (SST) turbulence model [17], the authors carried out comprehensive parametric analyses of the dependence of the lift reduction and drag increment of the S809 wind turbine airfoil [18] on the depth, surface density, surface extent, and location (distance from the leading edge) of the erosion pits. For all these parameters, critical values were determined above which the airfoil performance did not undergo any further significant reduction.

The studies above highlight that the interest in understanding and quantifying the dependence of wind turbine energy production on blade damage, particularly in the frequent case of damage due to leading edge erosion, is increasing. However, to the best of the authors' knowledge, there is presently no research into developing a reliable and rapid system for assessing such losses or tackling the challenges of developing this type of system for industrial application. The work presented in this paper aims at addressing this shortfall by presenting and demonstrating the modular wind turbine AEP loss prediction system (ALPS) framework, a novel data- , CFD- and engineering code-based technology for assessing wind turbine energy losses and load variations due to blade surface damage. The information made available by this technology can be used to *a*) quantify the revenue reductions due this type of AEP losses and help asset managers

deciding when it is most convenient to undertake maintenance, and *b*) assess the convenience of adopting safeguards such as leading edge protections [11, 19]. The rationale behind the development of ALPS is to provide a tool capable of rapidly and reliably assessing AEP losses due to real blade surface damages with a definition available in the form of three-dimensional (3D) images. Although ALPS has been designed to deal with fairly general surface damage pattern and severity, the demonstration provided in the study below focuses on the AEP losses of a multi-megawatt offshore wind turbine caused by moderate to advanced erosion-induced leading edge delamination.

The paper is structured as follows: the definition of the architecture, input and output data of ALPS, and the interdependencies of its modules are provided first; this is followed by the specification of the wind turbine computational aerodynamics subsystem, made up of the ANSYS FLUENT [20] incompressible RANS solver and the NREL wind turbine aerodynamics code AeroDyn [21]. The paper continues with the definition of the power control strategy of the turbine with nominal blade geometry. Then, the parametrization of the considered leading edge delamination damage, and the CFD set-up used for the generation of the force data of 2700+ damaged airfoils making up the initial ALPS database are presented. The machine learning (ML) approach used to extract from the ALPS airfoil repository the force data of the blade cross sections associated with user-given 3D damaged blade geometries is reported next. The Results section demonstrates the applicability of ALPS for real installations by using this novel technology to reliably estimate in a few seconds the power, loads and regulation curves of an offshore wind turbine whose blades feature a general leading edge delamination damage, representative of those observed in operation. In the same section, the formulation of a possible adaptive power control strategy of wind turbines with blade surface damage, aiming to mitigate the detrimental effect of this damage on AEP, is also presented and demonstrated. The concluding section summarizes this work and provides an overview of future extensions.

ENERGY LOSS PREDICTION SYSTEM

ALPS is a modular analysis framework consisting of several interlinked modules. Its main function is to determine the annual energy production of a wind turbine whose blades feature surface damage of general shape and severity. The modules of ALPS are indicated in the block diagram of Fig. 1, which shows with arrows module dependencies, and red boxes module outputs. The calculation of the wind turbine power and loads for the entire range of operating wind speeds relies on engineering code based on the blade element momentum theory (module labeled 'Wind Turbine Model'), which requires the lift and drag curves of the airfoils making up the cross sections of the considered damaged blade. The airfoil geometry and force database

of ALPS (box labeled 'Airfoil Database') contains geometry and force data of airfoils whose shape conforms to the nominal design intent or differs from that because of a blade surface damage developed and/or accrued during turbine operation. The airfoil data presently included in the ALPS database have been computed with NS CFD, but hybridization methods enabling the concurrent use of experimental and CFD airfoil force data will be investigated in forthcoming extensions.

The main input of ALPS is the current 3D geometry of the blades, consisting of the nominal geometry of the blade and any surface damage (box with enlarged view of delaminated blade leading edge), with the latter information typically available in the form of blade photographs. These data are passed to a geometry analysis system (GAS), which outputs sectional damage data (*e.g.* leading edge delamination extent and depth) for a user-given number of blade cross sections. The GAS module is built upon image processing and CAD software, and it is presently under development. In the ALPS demonstration considered below, the starting point is a set of blade airfoil leading edge delamination parameters selected on the basis of information available in the literature.

In general, none of the damaged airfoil profiles of an operational turbine will be contained in the current database. Therefore, ALPS uses a machine learning-based method to determine the lift and drag force data of each damaged airfoil making use of the knowledge repository of the airfoil database. In this study, an Artificial Neural Networks (ANNs) system is used to estimate the values of lift and drag for the whole operating range of the local angle of attack (AoA). The GAS module will include parametric representations of typical blade surface damage patterns, and, for each damaged cross section extracted from the monitored 3D blade geometry, will return the value of the parameters defining the damage of the associated airfoil. This set of parameters, along with a set of operation parameters of the blade sections (*e.g.* AoA range) form the input of the ANNs module, which returns force data over the requested range of operating conditions.

The force data of the damaged blade sections are then used by the wind turbine module to determine the power curve and the aerodynamic loads of the turbine being assessed. The alterations of the airfoil force data due to blade surface damage like erosion will also result in a variation of the optimal tip-speed ratio and the value of the blade pitch required to limit the power to its rated value above the rated wind speed. It is unclear whether wind turbine power control strategies can presently adapt all of their settings to account for these time-dependent (varying over several months) alterations, but it is expected they will, if they do not do so already. Therefore, in the study below the damaged turbine power control strategy yielding the optimal values of rotor speed below rated wind speed, and the value of the blade pitch limiting the power to its rated value above rated wind speed have been modified in order not to overestimate the AEP loss due to suboptimal turbine control. The modified or adaptive power control algorithm is set by the module labeled 'Control' in Fig. 1, and this modified control strategy is discussed later in the paper. The damaged turbine AEP is then computed by integrating the power curve of the damaged turbine against the wind frequency distribution at the turbine installation site.

WIND TURBINE COMPUTATIONAL AERODYNAMICS

For each operating condition, namely set values of wind speed, rotor speed and blade pitch, the aerodynamic power and rotor loads are determined with a blade element momentum theory (BEMT) code using as input also the lift and drag force data of the nominal or damaged airfoils corresponding to the rotor blade sections. The force data of the airfoils making up the blade under analysis are determined by means of the ANNs system, which, in turn, requires the force data of all airfoils in the ALPS database. The airfoil force data of the ALPS database are determined with Navier-Stokes CFD. The main features of the BEMT and CFD codes used in the analyses reported below are summarized in the following subsections.

Navier-Stokes computational fluid dynamics analysis

Version 19.2 of the finite volume CFD code ANSYS FLUENT [20] is used to determine the flow field and the forces of all considered nominal and damaged airfoils. To obtain these data, the incompressible RANS equations in pressure-based form are solved in conjunction with the $k - \omega$ SST eddy viscosity model for the turbulent closure using unstructured grids. The second order upwind scheme is used for the space-discretization of both the mean flow equations and the turbulence model equations. The adopted numerical integration is based on the *coupled* algorithm, whereby the momentum and the pressure-based continuity equations are solved in a fully-coupled fashion. The SST model equations are instead integrated in a segregated or loosely coupled fashion.

Blade element momentum theory analysis

The aerodynamic power and loads of turbines with nominal and damaged blade geometry for given value of wind speed, rotor angular speed and blade pitch are determined with AeroDyn [21], the NREL time-domain wind turbine aerodynamics module. Aerodynamic calculations within AeroDyn are based on the principles of actuator lines, whereby the 3D flow field around a slender body is approximated with a local 2D flow model past cross sections, and the distributed pressure and viscous stresses are approximated by lift forces, drag forces, and pitching moments lumped at the node associated with the considered 2D cross section. Using this approach, the code can compute aerodynamic loads on both rotor blades and turbine tower. Analysis nodes are distributed along the length of each blade and the
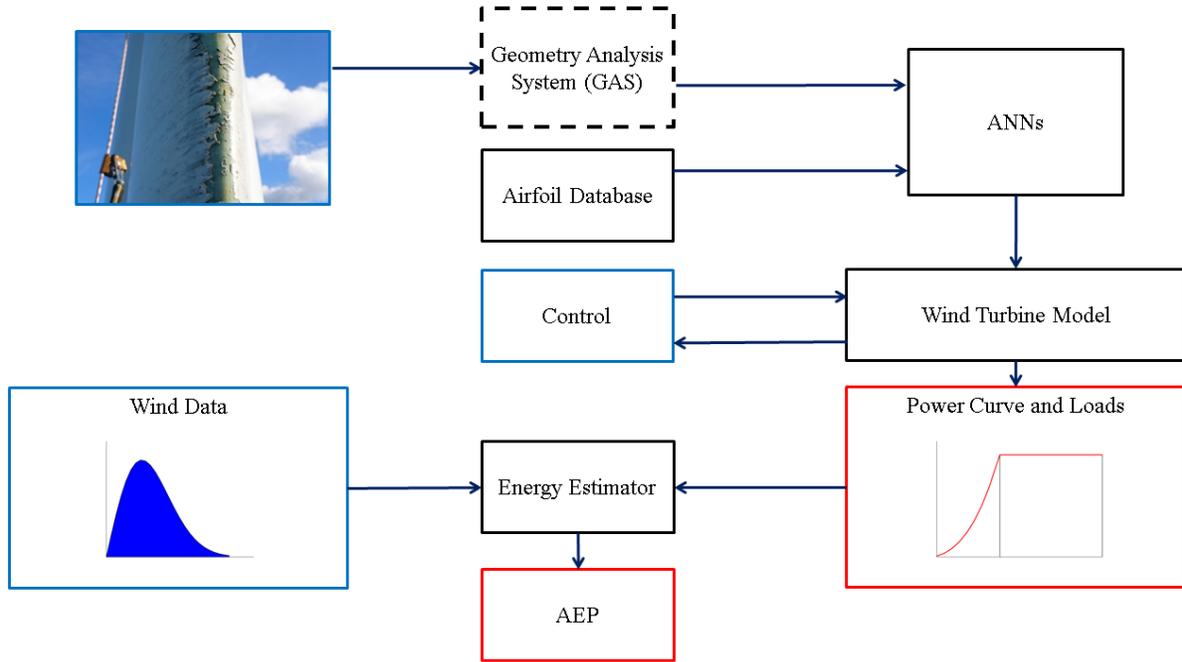
Figure 1. Definition of ALPS modules and their dependencies.

tower, the 2D forces and moment at each node are computed as distributed loads per unit length, and the total 3D aerodynamic loads are found by integrating the 2D distributed loads along the length of the considered blade or the tower.

AeroDyn consists of four submodels: *i*) rotor wake induction, *ii*) blade airfoil aerodynamics, *iii*) tower influence on blade aerodynamics, and *iv*) tower drag, and all four modules are used in the AeroDyn analyses reported in this study. For operating (*i.e.* not parked or idle) wind turbine rotors, AeroDyn calculates the influence of the rotor wake on blade aerodynamics via axial and circumferential induction factors based on the quasi-steady BEMT, which requires an iterative nonlinear solution process coupling modules *i*) and *ii*). By quasi-steady, it is meant that the induction reacts instantaneously to loading changes. The calculation of the induction factors and resulting inflow velocities and angles relative to the moving blade are based on the local flow field around each analysis node of the considered blade. The effects of local inflow skew, wind shear, turbulence, tower flow disturbances can also be included in the analysis. The Glauerts empirical correction with Buhls modification replaces the linear momentum balance at high axial induction factors. In AeroDyn, 3D flow features are either neglected or captured through corrections inherent in the model (*e.g.* Prandtl tip and hub loss corrections or skewed wake corrections) or the input data (*e.g.* rotational augmentation corrections applied to the airfoil force coefficients). The AeroDyn analyses reported below use steady uniform oncoming wind aligned with the rotor axis, *i.e.* no wind

shear and zero yaw error; the airfoil aerodynamics is assumed steady (*e.g.* no dynamic stall model is used), and the static pressure perturbation of the downwind tower on the blade aerodynamics is included.

WIND TURBINE CONTROL

The general strategy of the power control algorithm of utility-scale wind turbines aims at maximizing power by maximizing the power conversion efficiency between cut-in and rated wind speeds, and limiting power to the rated value between rated and cut-out wind speeds. In real applications there exist transitional regions before and between these two main regions. In this report, the general power control strategy developed for the NREL 5 MW reference turbine [14] is adopted. However, some alterations to this power control strategy are adopted for the turbine with damaged blade surfaces to avoid overestimating the AEP of these turbines by using the nominal power control settings, which do not maximize the performance of damaged turbines. These alterations are discussed in the Results section.

The profiles of turbine power P, low-speed shaft torque Q, angular speed Ω, tip-speed ratio (TSR) λ and blade pitch β against the wind speed U for a turbine with nominal blade shapes are reported in Fig. 2, in which the subscripts *c.i.*, R and *c.o.* denote respectively cut-in, rated and cut-out speeds. The turbine starts producing power once the wind speed reaches $U_{c.i.}$. In region 2, starting shortly after wind speed $U_{c.i.}$, the TSR λ
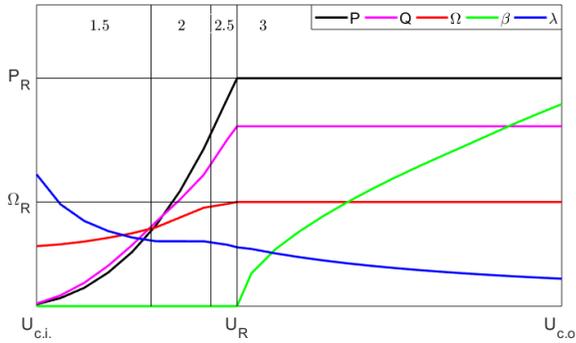
Figure 2. Wind turbine power control.

is kept constant and equal to the value yielding the maximum power coefficient, thus maximizing the harvested power. Therefore, Ω increases linearly with U, and the aerodynamic torque increases quadratically with both Ω and U in region 2. Region 2, however, is preceded by the transition region 1.5, in which the aerodynamic torque varies linearly with Ω, and Ω increases more slowly with U with respect to what occurring in region 2. Similarly, before the power reaches its rated value, the rotor speed starts increasing more slowly with the wind speed (region 2.5) than in region 2. This is because, also in region 2.5, the control algorithm enforces a linear relationship between Q and Ω. Until the rated wind U_R, the right boundary of region 2.5, is reached, the blade pitch β remains constant. As the wind speed increases above U_R, however, Ω remains constant, and the blades are actively pitched to feather by the amount required to reduce the lift and its projection on the rotor plane and maintain constant torque and power until the wind speed reaches $U_{c.o.}$, where the turbine is shut down.

AIRFOIL GEOMETRY AND FORCE DATA

The subsections below describe the procedure for generating the geometry of a large set of airfoils with delaminated leading edge making up the ALPS database used in this study, summarize the main numerical settings of the CFD analyses for determining the aerodynamic force coefficients of the damaged airfoils, provide verification and validation analyses of the adopted CFD methodology, and define the ML method used to determine the force data of damaged airfoils whose geometry is not included in the ALPS database.

Parametrization of leading edge delamination damage

The blade surface damage considered herein is leading edge delamination, an alteration of the leading edge region appearing more frequently in the advanced stages of leading edge erosion [2]. The geometry parametrization of leading edge delam-

ination adopted in this study is sketched in Fig. 3. The damage is defined by 3 parameters, namely its depth d, its upper side curvilinear length s_u, and its lower side curvilinear length s_l, both measured from the leading edge.
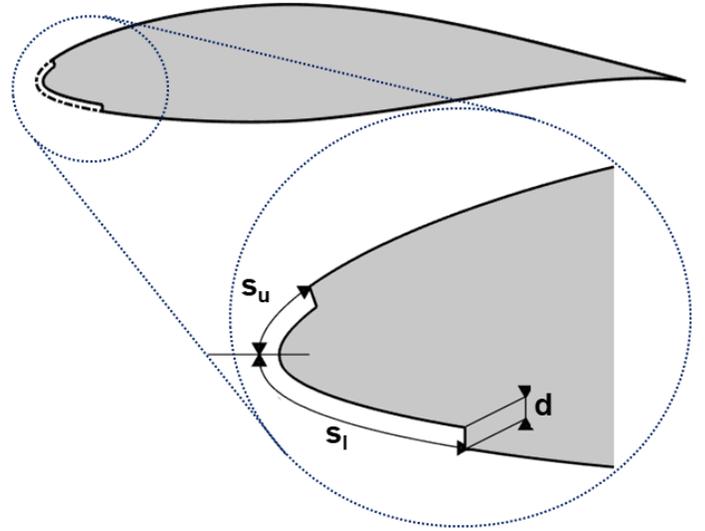

Figure 3. Geometric parametrization of leading edge delamination.

The baseline airfoils considered in this study are the 6 airfoils making up the cross sections of the NREL 5 MW reference turbine [14], namely the DU40-A17, DU35-A17, DU30-A17, DU25-A17, DU21-A17 and NACA64-A17 airfoils. The geometry of each of these airfoils is perturbed according to the value range of the delamination parameters reported in Tab. 3. For each delamination stage (mild, moderate and severe), the 3 parameters s_u, s_l and d are varied independently between the minima and maxima provided in the table with step Δ. All values are normalized by the airfoil chord c. Adopting the parameters reported in Tab. 3, 459 damaged shapes per nominal airfoil geometries are obtained, and the ALPS database has thus 2754 damaged airfoils. Each of these airfoils is generated by a MATLAB code that runs in serial mode on a desktop PC and takes just a few seconds to generate all geometry files.

CFD set-up

In this study, the aerodynamic forces acting on each nominal and damaged airfoil are determined using incompressible 2D NS CFD simulations with the ANSYS FLUENT software. A Reynolds number of 7 M, based on the airfoil chord and the magnitude of the relative velocity and similar to the spanwise averaged value of the NREL 5 MW turbine at rated wind speed, is

5

Table 1. Damage parameter choice for ALPS database.

	Mild			Moderate			Severe		
	min	max	Δ	min	max	Δ	min	max	Δ
$s_u/c \times 100$	0.1	1.0	0.1	1.3	3.1	0.2	3.6	9.9	0.7
$s_l/c \times 100$	1.2	3.0	0.2	3.3	10.5	0.8	10.5	22.2	1.3
$d/c \times 100$	0.1	0.1	-	0.2	0.8	0.2	1.0	2.0	0.2

adopted for all CFD simulations. For each airfoil, a sweep of 16 values of the AoA α, from -10° to 20° with a step of 2° is carried out. Structured C-grids were used in all cases. The C-shaped far field boundary is placed at about 45 chords from the airfoil. A velocity inlet far field boundary condition (BC) is applied on the front, lower and upper parts of the far field boundary, whereas a pressure outlet BC is applied on the rear part. The far field BC data for the SST model consist of a freestream turbulence intensity of 5 % and a turbulent-to-laminar viscosity ratio of 1. At the airfoil surface, a no-slip condition is enforced. No wall functions are used and the equations of the turbulence model are integrated all the way down to the wall boundary. The adopted wall distance of $3.9 \cdot 10^{-6}c$ of the grid nodes closest to the airfoil surface gives nondimensionalized minimum wall distance $y^+ \approx 1$ in all cases. All simulations of the ALPS database generated in this study model the flow as fully turbulent, and achieve a reduction of 4 to 5 orders of magnitude of the root-mean-square of both the mean flow equations and the two turbulence model equations. In the majority of the simulations this requires 2000 iterations, while in a few cases, up to 4000 iterations are required.

The grid past nominal airfoils features 151 grid nodes in the normal direction, 327 nodes along the airfoil surface, and a total of about 94K quadrilateral cells. The grid past airfoils with leading edge delamination differs from that past nominal airfoils because of an additional structured layer of cells filling the delaminated region. Because of this, these grids feature about 600 nodes along the airfoil and about 126K quadrilateral cells. These grid sizes were determined after comprehensive mesh refinement analyses, as summarized below. Views of the grid past the nominal and delaminated NACA64-A17 airfoil are reported in Fig. 4(a) and Fig. 4(b) respectively.

In the ALPS airfoil database generated for the demonstration reported in the Results section, a set of 16 AoAs is analyzed for each damaged airfoil, and the database generation thus requires $2754 \times 16 = 44064$ 2D FLUENT simulations. The process of generating the complete geometry of the physical domain, meshing it, running the CFD simulations is fully automated by means of MATLAB, JAVA, LINUX and ANSYS WorkBench scripting. The computationally most intensive task is the CFD simulation. For this reason, all these simulations are run on the Lancaster University HEC cluster [22]. Using 1 16-core HEC node, one

(a) Nominal airfoil geometry.
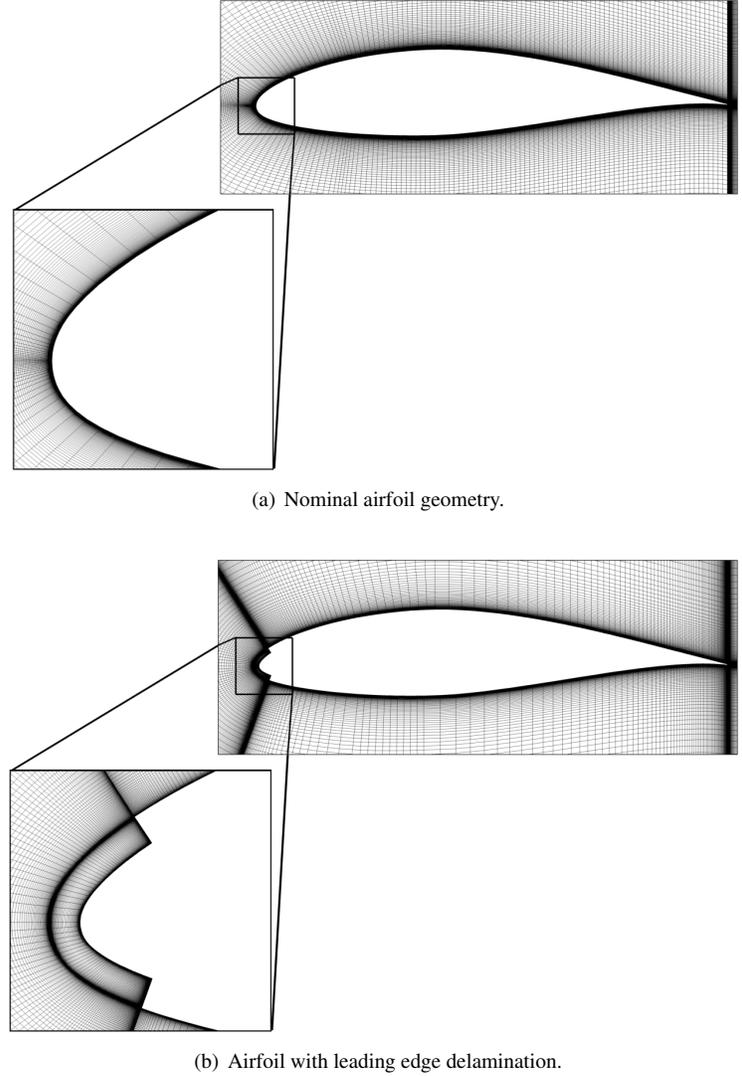

(b) Airfoil with leading edge delamination.

Figure 4. Enlarged views of computational grids past NACA64-A17 airfoil.

2D CFD simulation based on the grid settings reported above requires about 4 minutes of wall-clock time, and the construction of the lift and drag curves for each airfoil requires about 64 minutes of wall-clock time. Thus, the generation of the 2754-airfoil force database requires about 3525 hours of wall-clock time using one cluster node. However, the database generation is accomplished by using concurrently 20 cluster nodes, and the required wall-clock time is therefore reduced to about 1 week.

Verification and validation

Measured and computed force coefficients of the nominal NACA64-A17 airfoil between α=-10° and α=20° at a Reynolds

6

number of 6 M are reported in the two plots of Fig. 5. The CFD curves labeled 'coarse', 'medium' and 'fine' refer to structured grids featuring 26K, 94K and 320K quadrilateral cells respectively. The minimum wall distance in the medium refinement grid is $4.4 \cdot 10^{-6}c$, which gives nondimensionalized maximum wall distance $y^+ \approx 1$ for all AoAs at this Reynolds number. The minimum wall distance in the coarse and fine grids is respectively twice and half the medium grid value. Inspection of these CFD results shows that the medium and fine grid results differ negligibly from each other, confirming that the medium grid settings are adequate for the construction of the ALSP database. With regard to the comparison of grid-independent CFD results and experimental data, an excellent agreement of measured and computed c_l is obtained over the entire AoA range considered. An overall good agreement of computed and measured drag polars is also observed. All CFD results of Fig. 5 are obtained with the SST turbulence model enhanced by the $\gamma - Re_\theta$ transition model [23]. To achieve the good correlation of CFD and experimental data reported below, the constant a_1 appearing in the definition of the eddy viscosity had to be reduced from its default value of 0.31 to 0.28, similarly to the guideline in [4].

To further verify and validate the ALPS CFD set-up, the analysis of the aerodynamic forces acting on the DU96-W180 airfoil and a damaged variant of this profile at a Reynolds number of 1.5 M is considered next. The damaged variant is affected by leading edge delamination with damage parameters s_u/c=0.030, s_l/c=0.039 and d/c=0.00834, and is an approximation to one of the damaged variants of the DU96-W180 airfoil that were tested in a wind tunned [2]. Computed and measured force coefficients of the nominal and damaged airfoils are compared in Fig. 6, in which all measured data are those reported in [2]. Both CFD simulations use the same transtion model set-up of the nominal NACA64-A17 airfoil analysis, and a minimum wall distance of $1.6 \cdot 10^{-5}c$, which results in maximum y^+ of order 1 at all grid nodes around both airfoils. The nominal airfoil analyses in Fig. 6 use a C-grid with 94K quadrilateral cells, and those of the damaged airfoil use a modified C-grid with 126K elements. Both results are grid-independent. This was verified by carrying out the nominal airfoil simulations also with a coarse 26K-element grid and a fine 320K-element grid, and the damaged airfoil simulations also with a coarse 30K-element grid and a fine 400K-element grid. The curves in Fig. 6 highlight a fairly good agreement between simulations and experiments, particularly for AoAs up to about 8°. The general trends of CFD and measurements are in good agreement, including the prediction of the small negative AoA below which the lift of the damaged airfoil becomes slightly higher than that of the nominal airfoil. The general outcome of the comparison above is considered quite positive, also in light of some uncertainty on the CFD estimates due to insufficient information on the geometry of the damaged airfoil; moreover, it is noted that this airfoil is used in the outboard sections of turbine blades, where the AoA levels are rela-
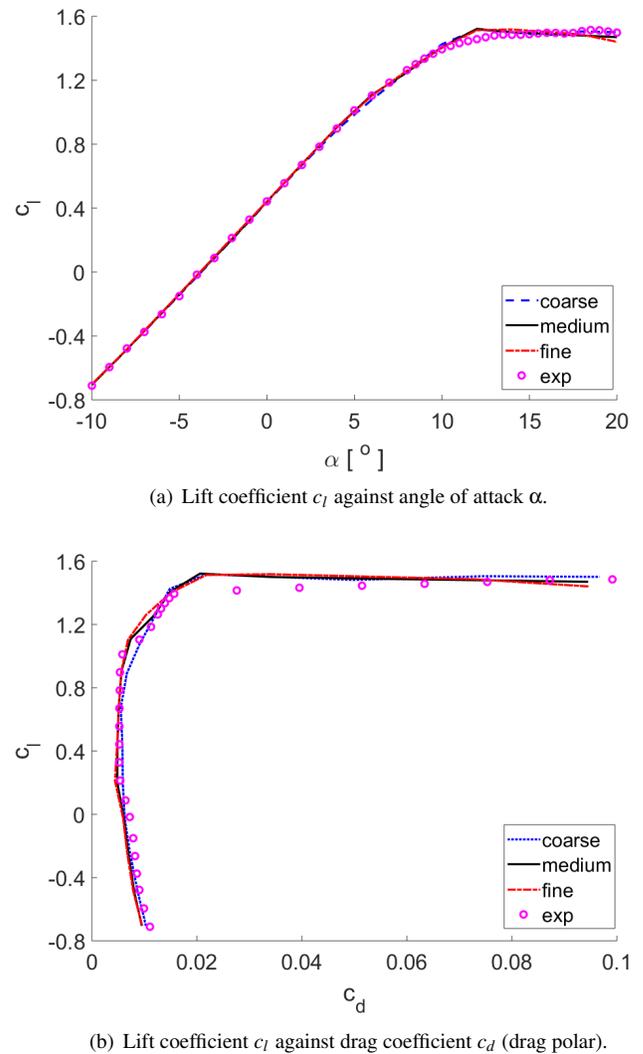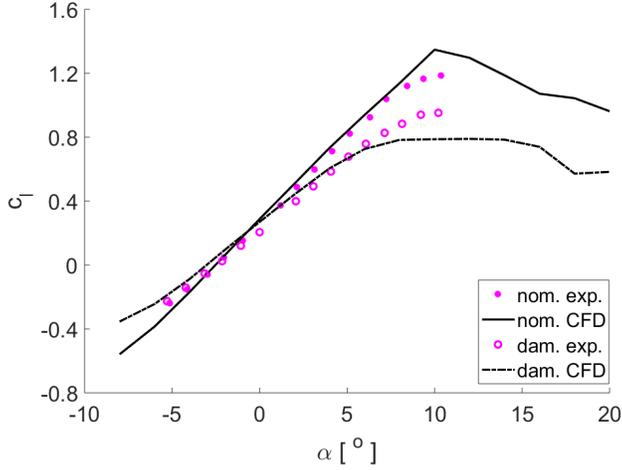

(a) Lift coefficient c_l against angle of attack α.

(b) Lift coefficient c_l against drag coefficient c_d (drag polar).

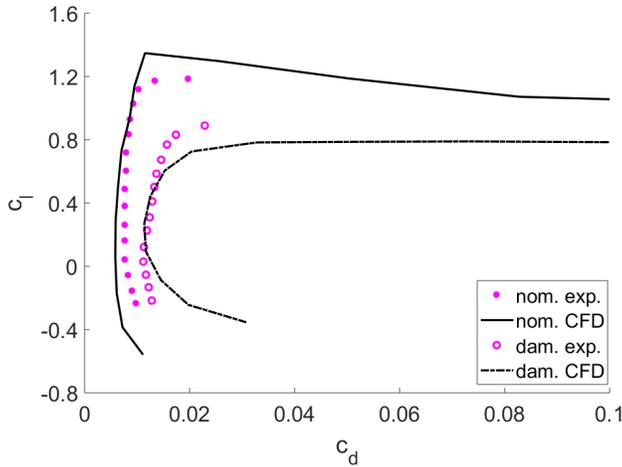Figure 5. Comparison of computed and measured force coefficients of NACA64-A17 airoil.

tively low, and are in the range in which the comparative analysis of nominal and damaged airfoil aerodynamics provides quite good results.

Machine learning approach

Machine learning consists of using algorithms and statistical models to develop computer systems that effectively perform a specific task without using explicit instructions, but rather relying on data patterns and inference. ML algorithms build a mathematical model based on given data sets (training data) to make predictions without being explicitly programmed to perform the task. In this study, ML is used to develop a mathematical model providing rapid estimates of the eroded airfoil

(a) Lift coefficient c_l against angle of attack α.

(b) Lift coefficient c_l against drag coefficient c_d (drag polar).

Figure 6. Comparison of computed and measured force coefficients of nominal and damaged DU96-W180 airoil.

force coefficients without solving the Navier-Stokes equations by means of time-consuming CFD simulations. Generic multi-layer perception (MLP) feed-forward Artificial Neural Networks with one hidden layer are used in ALPS to learn from the lift coefficient c_l and the drag coefficient c_d data patterns in the ALPS database of damaged airfoils, and infer the aerodynamic forces of eroded airfoils not contained in the database. One c_l and one c_d ANNs model is contructed for each of the 6 airfoils making up the blade of the NREL 5 MW turbine.

Single layer MLPs like those used herein consist of universal function approximators $\mathbf{f_g}(\mathbf{x}) : \mathbb{R}^{n_d} \to \mathbb{R}^{n_o}$ [24], where n_d is the size of the input vector $\mathbf{x}$, and n_o is the size of the output vector function $\mathbf{f_g}$. In the present ALPS version, $\mathbf{x} =$ $(s_u/c, s_l/c, d/c, \alpha)^T$ and $n_d = 4$, whereas $n_o = 1$ since the output function is scalar, corresponding to either c_l or c_d. The general matrix-vector definition of $\mathbf{f_g}$ is:

$$\mathbf{f_g}(\mathbf{x}) = A2(\mathbf{b}^{(2)} + \mathbf{W}^{(2)}(A1(\mathbf{b}^{(1)} + \mathbf{W}^{(1)}\mathbf{x}))) \qquad (1)$$

where $\mathbf{W}^{(1)}$ is a weight matrix of size $(N \times n_d)$ and N is the number of *neurons* on the hidden layer, $\mathbf{b}^{(1)}$ is a bias (column) vector of length N, $\mathbf{W}^{(2)}$ is a weight matrix of size $(n_o \times N)$, $\mathbf{b}^{(2)}$ is a bias (column) vector of length n_o, and $A1$ and $A2$ are the activation functions of the hidden layer and the output layer respectively. The general schematic of one-layer MLP feed-forward ANNs systems, like that used in the present ALPS release, is depicted in Fig. 7.
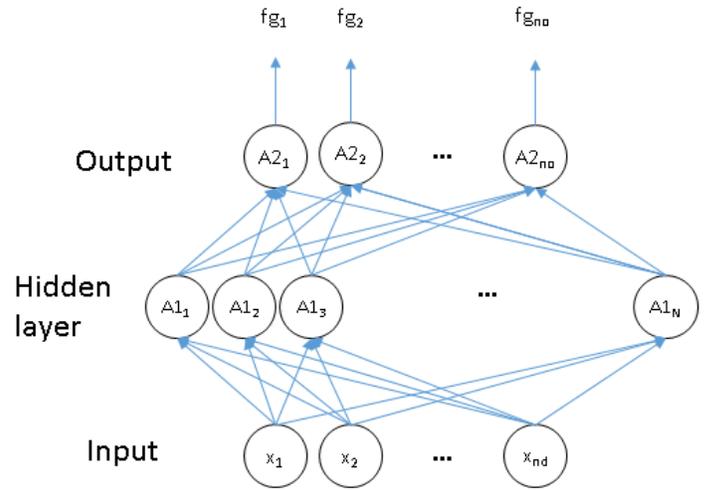

Figure 7. General schematic of one-layer MLP feed-forward ANNs systems.

Typically, $A1$ is the hyperbolic tangent sigmoid function defined as $tanh(a) = (e^a - e^{-a})/(e^a + e^{-a})$, and $A2$ is linear. With this choice, function $\mathbf{f_g}(\mathbf{x})$ becomes:

$$\mathbf{f_g}(\mathbf{x}) = \mathbf{b}^{(2)} + \mathbf{W}^{(2)}(tanh(\mathbf{b}^{(1)} + \mathbf{W}^{(1)}\mathbf{x})) \qquad (2)$$

Given a set of N_s training samples $\{(\mathbf{x}_1, \mathbf{y}_1), \ldots, (\mathbf{x}_{N_s}, \mathbf{y}_{N_s})\}$, where $\mathbf{y}_i$ is the observed response to the input $\mathbf{x}_i$, a learning algorithm seeks the values of the weight matrices and bias vectors that minimize the difference between part or all of the observed N_s sample responses $\mathbf{y}_i$ and the N_s responses given by $\mathbf{f_g}(\mathbf{x}_i)$. Gradient-based optimization is often used to determine

the weight matrices and the bias vectors by minimizing the aforementioned difference. In this circumstance, since the responses are assumed to be smooth functions of the inputs $\mathbf{x}_i$ and the internal weights and biases, the gradients with respect to weights and biases of the difference between sample responses and ML approximations can be computed using the so-called backpropagation method, which essentially relies on applying the chain rule for derivation. The backpropagation approach can be applied repeatedly to propagate gradients through all layers starting from the output at the top, where the network gives its response, and working all the way down to the bottom (hidden layer), where the input is provided. Once the gradients with respect to weights and biases for each layer are computed, the objective function expressing the level of fitting of the training data can be optimised.

If the ANNs system has a sufficiently high number of neurons or degrees of freedom in the hidden layer, a parameter proportional to the chosen number of neurons, the fitting error can be reduced to machine zero; this results in the system *overfitting* the training data, and being possibly unable to generalize adequately its predictions to regions of the input space where there are no or insufficient training data. To mitigate this risk, two different approaches have been adopted in this study. One approach consists of subdividing the available data set into a training set and a validation set. At each step of the gradient-based optimization via backpropagation (training), the fitting error based on the validation set is also computed. The system training is then stopped when the fitting error based on the validation set starts increasing. This typically happens before the fitting error based on the training set achieves machine zero. The alternative approach introduces one or more *regularization* terms that modify the fitting function so that the obtained ANNs system has good generalization properties. One of the most widely used regularization approaches is Bayesian regularization, in which a modified linear combination of fitting errors, weights and biases is minimized [25].

Using either learning approach to prevent overfitting, the learning process via backpropagation consists of a local gradient-based optimization problem, which is solved with the Levenberg-Marquardt (LM) method [26]. Because of the local nature of the method, however, the learning outcome can be affected by the process initialization. To reduce the likelihood of this occurrence, 100 training runs with different random initializations are carried out both with the training and validation set approach, and the Bayesian regularization approach. Moreover, this is done with different values of N in both cases to determine the value of this parameter that maximizes the predictive capabilities of the ANNs system. In this study, the size of the training set is 95 % of the randomized database when using Bayesian regularization, and the remaining 5 % forms the test set, used to test the generalization strength of the ANNs system. The size of the training set is instead 80 % of the randomized database and that of the validation set is 15 % of the same database when using the approach without regularization, and the remaining 5 % forms the test set. The ANNs system selected for the force coefficients of each of the 6 sets of damaged airfoils is that with high fitting of the training set and good generalization on the test. The typical optimal value of N for both the lift and force coefficients of the ANNs system of the 6 airfoils is found to vary between 60 and 500.

RESULTS

To demonstrate the use of ALPS for industrial problems, a moderate to severe leading edge delamination affecting the blades of the NREL 5 MW reference turbine is considered. The damage is assumed to affect the entire length of the blade, and to have irregular edges (variable s_u and s_l) and variable depth d. It is also assumed that the geometry of the delamination damage is the same for all three blades. Different delamination patterns on each blade, however, could be analyzed by means of the same approach adopted in [27] to analyze the impact on the mean and standard deviation of the turbine power of normally distributed deviations of the blade outer shape from the nominal geometry due to finite manufacturing tolerances. In that study, the performance of a three-blade rotor whose blades are not identical is obtained by taking the arithmetic average of the performance (power and loads) of three different fictitious rotors, each with identical blades affected by a different pattern of blade geometry errors.

The leading edge damage considered herein has different values of delamination parameters s_u/c, s_l/c and d/c over 25 radial segments or strips of the blade. The minimum, maximum and mean (μ) values and the standard deviation (σ) of the delamination parameters s_u, s_l and d of the damage analyzed below are reported in columns 2-4 of Tab. 2, in which all values are normalized by the airfoil chord c. A 3D view of the considered delamination pattern is provided in Fig. 8, in which US denotes the view of the blade upper side, and LS that of the blade lower side.

Table 2. Main geometric values of analyzed blade damage.

	min	max	μ	σ
$s_u/c \times 100$	1.28	8.2	5.6	1.5
$s_l/c \times 100$	1.7	12.2	7.1	1.9
$d/c \times 100$	0.65	1.26	0.85	0.22

To assess the reliability of the ANNs system based on the ALPS database, the comparison of the lift and drag coefficient curves obtained using CFD and the selected ML approach at six
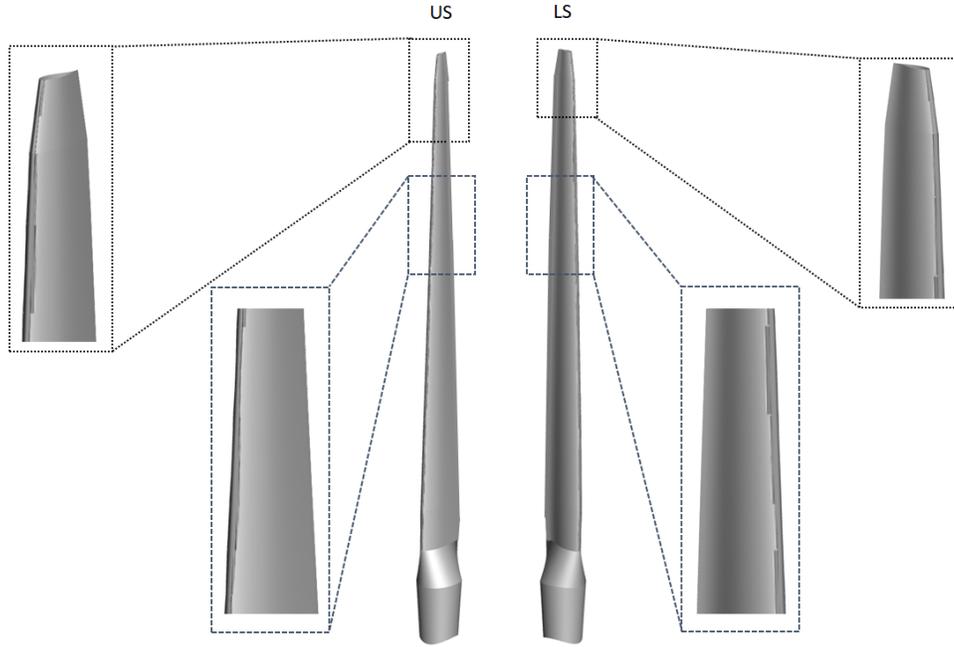
9

Figure 8. 3D view of analyzed leading edge erosion damage.

radial positions is considered next. The value of the radius r of the 6 blade cross sections normalized by the rotor tip radius R is reported in the second row of Tab. 3, and the chord-normalized values of s_u, s_l and d of each section are reported below the corresponding value of r/R. The curves of lift coefficient c_l and drag coefficient c_d from $-10°$ to $20°$ of the six sections are depicted in the twelve subplots of Fig. 9. Each subplot provides 3 curves for the considered force coefficient, namely that of the delaminated section obtained using a CFD analysis (curve labeled CFD-d), that of the delaminated section obtained using the ANNs system (curve labeled ANN-d), and that of the nominal section obtained using a CFD analysis (curve labeled CFD-n). With regard to the ANNs prediction reliability, an overall excellent agreement between the CFD and ANNs predictions of the force coefficients is observed. Some small discrepancies between the two predictions are observed only at the lowest AoA values of the DU35-A17 and NACA64-A17 airfoils. The most likely cause for this is the need for further optimization of the ANNs set-up, which may require altering the number of ANNs neurons and/or recalibrating the weights determining the amount of training using the central and end regions of the considered AoA interval. In practice, the aforementioned small discrepancies do not affect the analyses below, since they occur for damaged airfoils which do not operate in the highlighted AoA range. With regard to computational cost, it is noted that obtaining the six pairs of c_l and c_d curves by means of ML, starting from the three delamination parameters

of the six damaged airfoils, requires just a few seconds. Conversely, obtaining the same force data using CFD requires about 72 minutes of wall-clock time, resulting from 8 minutes to generate 6 grids using concurrently 6 processor cores, and 64 minutes for determining 6 lift and drag curves with 2D CFD simulations using concurrently 6 16-core HEC nodes.

Cross-comparing the force coefficient curves of the damaged and nominal airfoils also shows that for all cross sections $a)$ the magnitude of the lift coefficient of the eroded airfoils at low and high AoA is lower than that of their nominal counterparts, but is comparable to that of the nominal airfoils for AoA α between about $-5°$ and $5°$, and $b)$ a qualitatively similar pattern is observed for the drag coefficients, and the difference between the mean drag coefficient of the damaged and nominal airfoils increases as the blade thickness decreases, $i.e.$ as the blade radius increases.

The curves of the turbine power P, torque Q and thrust T against the freestream wind speed U of the damaged and nominal turbines are compared in Fig. 10(a), whereas those of the rotor speed Ω, the blade pitch β and the TSR λ of the same turbines are compared in Fig. 10(b). An excellent agreement between the power, load and regulation curves of the turbine with blade leading edge delamination obtained using either CFD or ANNs airfoil data is observed. It is noted that, once the damaged airfoil lift and drag data are determined using the output of relatively lengthy direct CFD simulations or the substantially faster ML
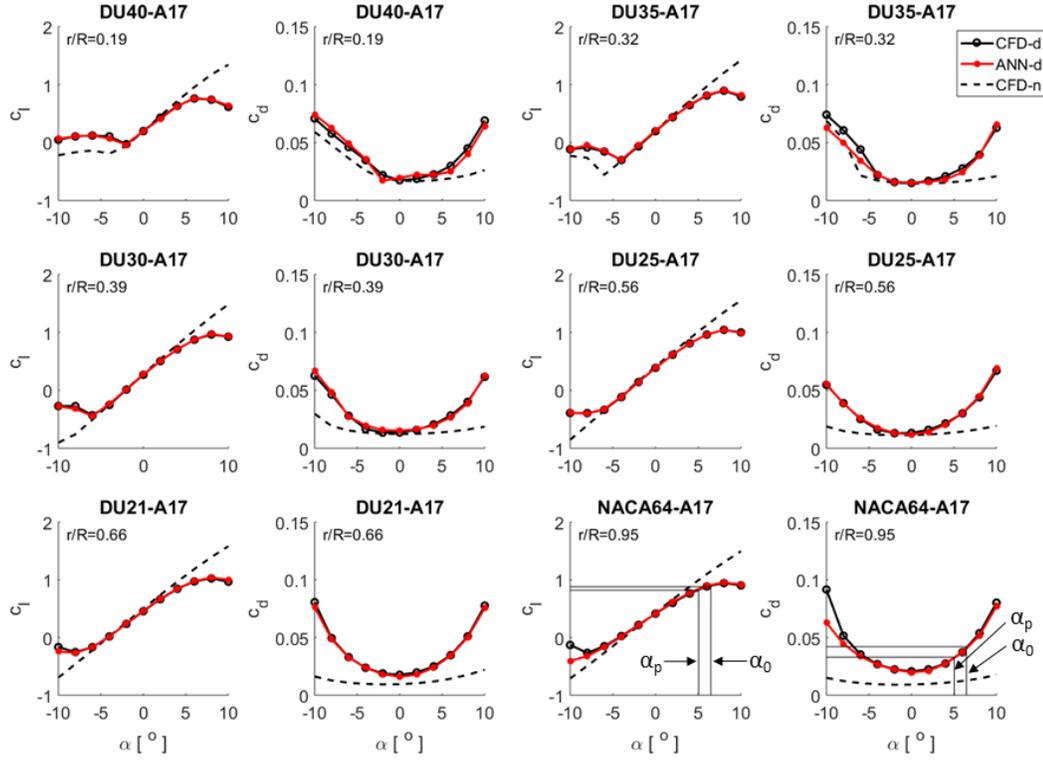
10

Figure 9. Comparison of lift and drag forces of nominal and damaged airfoils at six radial positions.

Table 3. Damage geometry parameters at six radial positions.

	r/R					
	0.19	0.32	0.39	0.56	0.66	0.95
$s_u/c \times 100$	7.1	6.8	4.3	5.5	3.9	4.0
$s_l/c \times 100$	7.5	7.4	4.9	6.3	9.0	7.6
$d/c \times 100$	0.66	0.66	0.66	0.66	0.78	1.2

approach, the generation of both curve sets requires just a few seconds. For determining the regulation curves of the turbine affected by the given leading edge damage, AeroDyn requires lift and drag data for 27 airfoils, corresponding to the airfoils at the mean radius of the 25 blade strips, the aerodynamic section at the lowest blade radius and the tip section. The direct CFD method for determining the force data of the 27 airfoils requires a wall-clock time of 136 minutes, resulting from 8 minutes for generating the CFD grids and 128 minutes to run 27 CFD analyses, each for 16 values of α, using concurrently 20 16-core HEC nodes. Using the ANNs system, conversely, requires just a few

seconds.

The power control strategy adopted for the turbine with damaged blades is similar to that used for the turbine with nominal blade geometry, but its target settings are adapted to the new rotor aerodynamic characteristics resulting from the sectional force alterations of the blades. To determine the adaptive control settings, the rated aerodynamic power of 5.30 MW, the minimum rotor speed of 6.9 RPM, the maximum rotor speed of 12.1 RPM and the cut-off wind speed of 25 m/s of the nominal turbine are adopted also for the turbine with eroded leading edges. Because of the differences of the lift and drag curves of the nominal and eroded airfoils highlighted above, however, the cut-in and rated wind speeds of the damaged and nominal turbines are slightly different: the cut-in and rated wind speeds of the nominal turbine are 3.0 and 11.4 m/s respectively, whereas those of the damaged turbine are 3.5 m/s and 14.0 m/s respectively. For both turbines, a linear relation between torque and rotor speed is enforced in region 1.5, and such linear relation is maintained until Ω increases by 30 % over the cut-in value. At the end of region 1.5, Ω=9.0 RPM for both turbines, but U=7.7 m/s for the nominal turbine and U=7.3 m/s for the damaged turbine. For the nominal turbine, the rotor speed in the following

region 2 is set to the value corresponding to the known optimal value of λ=7.55 [14], and, once Ω achieves 90 % of its maximum value (Ω=11.6 RPM) at U=10.3 m/s, the control uses again a linear relation between torque and rotor speed (region 2.5) until the rated power and maximum rotor speed are achieved at the rated wind speed of 11.4 m/s. Once the rated power has been achieved, the blade pitch starts increasing to reduce AoAs and maintain the power equal to its rated value as the wind speed increases until the cut-off wind speed.

For the damaged turbine, the rotor speed in region 2 is set to the value that maximizes the aerodynamic power for each wind speed. This is achieved by wrapping AeroDyn with a MATLAB script that for each wind speed uses the golden section search [28] for gradient-based optimization to determine the optimal value of the rotor speed. This operation is required because the values of the optimal TSR (and also that of the corresponding maximum power coefficient) of the damaged and nominal turbines are different. The optimal operation parameters of the former turbine are unknown, and they also vary during operation as erosion progresses. Tracking the optimal TSR of the damaged turbine as U increases, one finds that this turbine achieves the maximum rotor speed of 12.1 RPM at U=10.0 m/s, well before the rated wind speed of the nominal turbine. Therefore, from U=10.0 m/s to U=11.4 m/s, the rotor speed of the damaged turbine is kept constant and equal to its maximum value. At 11.4 m/s, however, the aerodynamic power of the damaged turbine is still significantly lower than the rated power. To achieve more rapidly the rated aerodynamic power as the wind speed increases above 11.4 m/s, it is found that it is beneficial to start pitching to feather the eroded blades. At a first glance, this seems counterintuitive. The reason for this occurrence is that reducing the AoA at the outer sections of the eroded blade results in the consequent drag reduction outweighing the corresponding lift reduction, and thus in slightly larger torque at lower AoA. This is illustrated in the lift and drag curves of the blade section at r/R=0.95 in Fig. 9. The two values of the AoA labeled $α_p$ and $α_0$ in these subplots are respectively the values computed by AeroDyn using the blade pitch that maximizes power and no pitch at U=12 m/s. It is seen that at $α = α_p$ a significantly lower drag than at $α = α_0$ can be obtained. As mentioned, the lift coefficient at $α = α_p$ is lower than at $α = α_0$, but due to low twist of the outboard blade sections the reduction of the drag outweighs that of the lift, resulting in an overall higher torque. At 14 m/s, the damaged turbine achieves the rated aerodynamic power. For U varying between 11.4 to 14.0 m/s, the blade pitch that maximizes the aerodynamic power is obtained by wrapping AeroDyn with a MATLAB script that for each wind speed uses the golden section search to determine the optimal blade pitch. Increasing the wind speed above the rated value of 14 m/s requires more significant increments of the blade pitch to maintain the power to its rated level. Between the rated and the cut-out wind speed, AeroDyn is wrapped by a MATLAB script that uses Newton's method to determine the blade pitch yielding the rated aerodynamic power.

The AEP loss due to the considered damage is assessed by considering a site with mean wind speed of 9.36 m/s over one year, and featuring a Rayleigh wind frequency distribution. These wind data are representative of offshore sites on the north-western coast of England. Integrating the power curve of the nominal and damaged turbines against this wind frequency distribution and ignoring down-times of both turbines, gives AEP values of 22163 MWh and 20345 MWh. This corresponds to an AEP loss of 8.2 %, a value of the same order of magnitude of those reported in the literature. It has also been verified that the AEP loss of the damaged turbine obtained by ignoring its optimal TSR alterations (*i.e.* adopting the nominal dependence of the rotational speed on the wind speed from cut-in to cut-out but allowing the pitch controller to limit the aerodynamic power to a constant value of 5.3 MW above rated wind speed) are 16.7 % of the nominal AEP, twice the loss obtained with the adaptive power control discussed above.

With regard to structural loads, it is noted that the rotor thrust of the nominal turbine reaches a maximum at the rated operating point ($U = 11.4$ m/s) before dropping again. This peak is typical of variable generator speed variable blade-pitch-to-feather wind turbines because of the transition that occurs in the control system at rated speed between the active generator torque and the active blade pitch control regions. On the other hand, for the considered power control strategy of the damaged turbine, one notes that *a*) a fairly flat region of the thrust between the wind speed where the blade pitch starts increasing ($U = 11.4$ m/s) and that at which the rated power is achieved ($U = 14.0$ m/s) exists, and *b*) the thrust of the damaged turbine is higher than that of the nominal turbine even before the former reaches rated power, and remains such until the cut-off wind speed.

CONCLUSIONS

This study has presented ALPS, a novel modular technology for assessing wind turbine energy losses due to blade surface damage. The wind turbine power curve is determined by using engineering codes based on BEMT, such as the NREL FAST and AeroDyn codes. The force coefficients of the damaged airfoils associated with the cross sections of the blades with general leading edge delamination due to erosion are determined rapidly using an artificial neural networks system trained using a pre-existing database of damaged airfoil shapes containing airfoil force coefficients for the whole working range of AoAs. The presented demonstration focused on a radially irregular leading edge delamination of the blades of the NREL 5 MW turbine, and the analyses revealed that the considered damage of moderate to severe level, reduces the turbine AEP by about 8 %, a considerable amount which is also in line with other measured and computed estimates in the literature. The power control strategy of the damaged turbine was modified between rated and cut-in wind speeds
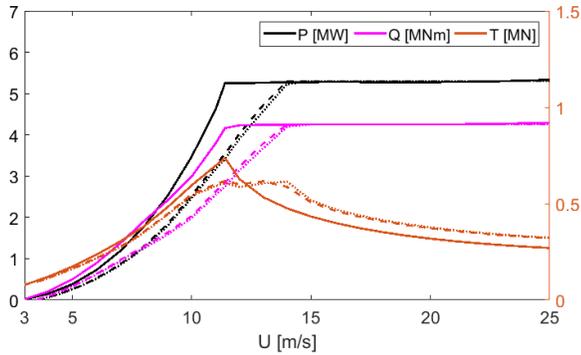
(a) Power (P), torque (Q) and thrust (T) against wind speed (U).
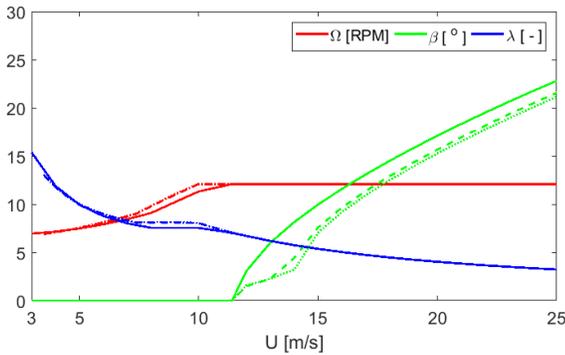
(b) Rotor speed (Ω), blade pitch (β) and TSR (λ) against wind speed (U).

Figure 10. Steady state performance and control curves. Solid, dotted and dashed lines refer respectively to analysis of turbine with nominal blade geometry, damaged blade surface using CFD, and damaged blade surface using ML.

to ensure maximum power also for the damaged turbine. This alteration is needed due to the different optimal TSR of the nominal and damaged turbines. In the case of power controllers lacking this adaptive strategy, thus not accounting for the reduction of the blade aerodynamic efficiency as wear and erosion progress during operation, the actual AEP loss is expected to be higher, up to twice the value recorded using adaptive control. With respect to this, the presented study provides some guidelines on how to make power control more robust to the time-dependent deterioration of the aerodynamic efficiency of the blades.

In the presented demonstration, the ALPS database is generated using 2D Navier-Stokes incompressible flow simulations of the ANSYS FLUENT CFD code. By automating the geometry and mesh generation phases, the execution of the CFD analyses and the collection of the airfoil force data by means of MATLAB, JAVA, LINUX and ANSYS WorkBench scripting, and by using 20 16-cores nodes of the HEC cluster, the 44064 simulations required to determine the lift and drag curves of 2754 damaged airfoils have been carried out in about one week of

wall-clock time. Once the database has been completed, however, the energy loss of wind farms consisting of hundreds of turbines featuring general blade surface damages not included in the database can be determined in a few minutes at any time of the 25-year lifetime of the wind farm thanks to the extremely low computational cost of the ML estimates and the BEMT-based engineering analyses. A practical issue in the ALPS applicability may arise when the nominal blade geometry is unavailable to the wind farm operator and/or turbine maintenance provider, since this may hinder the generation of the damaged airfoil geometries required to build the airfoil force database. This difficulty may be circumvented by basing the entire damage analysis on a turbine of known geometry, and overall design, control and rated power broadly comparable to the operational turbine under consideration, assuming that the percentage AEP loss is comparable. A second aternative consists of using reverse engineering to obtain an approximation to the nominal blade geometry. It is also noted, however, that the trend of wind turbine manufacturers also providing servicing to wind farm operators is rapidly increasing. This occurrence removes the geometry accessibility issue, since these service providers can use ALPS on behalf of wind farm operators to better inform cost analyses and blade material-related choices. In all cases, once the nominal blade geometry is available, the damaged airfoil database generation is a fairly straighforward and inexpensive process, which can be made even more accessible by using open-source software and cloud computing.

The presented study considered only the delamination pattern of the leading edge damage caused by erosion. In the generation of the ALPS database, the impact of earlier-stage pit and gouge damage patterns can be also analyzed by replacing the 2D NS CFD simulations with 3D simulations of radially thin constant-chord blade slices featuring different sizes and distributions of these 3D damage patterns. The impact of variable-roughness along damaged blade surfaces can also be accounted for using custom-tailored wall boundary conditions.

Finally, the geometry analysis system module in Fig. 1 was not needed in the presented demonstration, since the ALPS analysis started from the knowledge of the damaged blade sections, rather than from surface definitions of the blade damage. In field applications, the geometry of the damaged blade sections will be provided by GAS, the key link between the damaged blade photographs made available by the condition monitoring provider and ALPS; the GAS implementation will be reported in forthcoming studies.

ACKNOWLEDGMENT

itoring prompted this research programme.

REFERENCES

[1] 3M, 2011. A 3M Study Is the First to Show the Effects of Erosion on Wind Turbine Efficiency. `https://www.pressebox.com/pressrelease/3m-deutschland-gmbh/a-3m-study-is-the-first-to-show-the-effects-of-erosion-on-wind-turbine-efficiency/boxid/445007`. Accessed on 6 May 2019.

[2] Sareen, A., Sapre, C.A., and Selig, M.S., 2014. "Effects of leading edge erosion on wind turbine blade performance". *Wind Energy, 17*(10), pp. 1531–1542.

[3] Khalfallah, M.G., and Koliub, A.M., 2007. "Effect of dust on the performance of wind turbines". *Desalination, 209*, pp. 209–220.

[4] Zanon, A., De Gennaro, M., and Kuehnelt, H., 2018. "Wind energy harnessing of the NREL 5 MW reference wind turbine in icing conditions under different operational strategies". *Renewable Energy, 115*, pp. 760–772.

[5] Jasinski, W.J., Noe, S.C., Selig, M.S., and Bragg, M.B., 1998. "Wind turbine performance under icing conditions". *Journal of Solar Energy Engineering,, 120*(1), pp. 60–65.

[6] Bak, C., Andersen, P.B., Madsen, H.A., and Gaunaa, M., 2008. Design and Verification of Airfoils Resistant to Surface Contamination and Turbulence Intensity. AIAA paper 2008-7050, August. 26th AIAA Applied Aerodynamics Conference, Honolulu, Hawaii.

[7] Corten, G.P., and Veldcamp, H.F., 2001. "Aerodynamics: Insects can halve wind-turbine powers". *Nature Brief Communications, 412*, pp. 41–42.

[8] van Rooij, R.P.J.O.M., and Timmer, W.A., 2003. "Roughness Sensitivity Considerations for Thick Rotor Blade Airfoils". *Journal of Solar Energy Engineering, 125*(4), November.

[9] Somers, D.M., 2004. The S814 and S815 Airfoils. Tech. Rep. NREL/SR-500-36292, NREL, Golden, CO, USA, December.

[10] Fuglsang, P., and Bak, C., 2004. "Development of the Risø wind turbine airfoils". *Wind Energy, 7*(2), pp. 145–162.

[11] Schramm, M., Rahimi, H., Stoevesandt, B., and Tamgager, K., 2017. "The Influence of Eroded Blades on Wind Turbine Performance Using Numerical Simulations". *Energies, 10*(9), pp. 1–15.

[12] OpenCFD Ltd. OpenFOAM - The Open Source Computational Fluid Dynamics (CFD) Toolbox. `www.openfoam.org`. Accessed on 6 May 2019.

[13] Jonkman, J. FAST: An aeroelastic computer-aided engineering (CAE) tool for horizontal axis wind turbines. `https://nwtc.nrel.gov/FAST`. Accessed on 6 May 2019.

[14] Jonkman, J., Butterfield, S., Musial, W., and Scott, G., 2009. Definition of a 5-MW Reference Wind Turbine for Offshore System Development. Tech. Rep. NREL/TP-500-38060, NREL, Golden, CO, USA.

[15] Troen, I., and Petersen, E., 1989. European Wind Atlas. Technical Report, ISBN 87-550-1482-8, Risø National Laboratoy, Roskilde, Denmark.

[16] Wang, Y., Hu, R., and Zheng, X., 2017. "Aerodynamic Analysis of an Airfoil with Leading Edge Pitting Erosion Evolutionary Computation". *Journal of Solar Energy Engineering, 139*(6).

[17] Menter, F.R., 1994. "Two-Equation Eddy-Viscosity Turbulence-Models for Engineering Applications". *AIAA Journal, 32*(8), August, pp. 1598–1605.

[18] Somers, D.M., 1997. Design and Experimental Results for the S809 Airfoil. Tech. Rep. NREL/SR-440-6918, NREL, Golden, CO, USA.

[19] Giguere, P., and Selig, M.S., 1999. "Aerodynamic Effects of Leading-edge Tape on Airfoils at Low Reynolds Numbers". *Wind Energy, 2*, pp. 125–136.

[20] Ansys-Inc, 2019. Fluent theory guide, release 19.2. `https://www.ansys.com/Products/Fluids/ANSYS-Fluent`. Accessed on 6 May 2019.

[21] Heyman, G., Jonkman, B., Murray, R., Damiani, R., and Jonkman, J. AeroDyn: a time-domain wind and MHK turbine aerodynamics module. `https://nwtc.nrel.gov/AeroDyn`. Accessed on 6 May 2019.

[22] Lancaster University. High End Computing (HEC). `www.lancaster.ac.uk/iss/hec`. Accessed on 6 May 2019.

[23] Menter, F.R., Langtry, R.B., Likki, S.R., Suzen, Y.B., Huang, P.G., and Völker, S., 2006. "A Correlation-Based Transition Model Using Local Variables - Part I: Model Formulation". *Journal of Turbomachinery, 128*(3), July, pp. 413–422.

[24] Cybenko, G., 1989. "Approximation by superpositions of a sigmoidal function". *Mathematics of Control, Signals, and Systems, 2*, pp. 303–314.

[25] MacKay, D., 1992. "Bayesian Interpolation". *Neural Computation, 4*, pp. 415–447.

[26] Hagan, M.T., and Menhaj, M., 1994. "Training feedforward networks with the Marquardt algorithm". *IEEE Transactions on Neural Networks, 5*, pp. 989–993.

[27] Campobasso, M.S., Minisci, E., and Caboni, M., 2016. "Aerodynamic design optimization of wind turbine rotors under geometric uncertainty". *Wind Energy, 19*(1), pp. 51–65.

[28] Giordano, F.R., Fox, W.P., Horton, S.B., and Weir, M.D., 2009. *A First Course in Mathematical Modeling*. Brooks/Cole, 511 Forest Lodge Rd Pacific Grove, USA.